International Journal of Plasticity 81 (2016) 196–208

Contents lists available at ScienceDirect

International Journal of Plasticity

journal homepage: www.elsevier.com/locate/ijplas

Statistically motivated model of mechanisms controlling evolution of deformation band substructure

Jan Kratochvíl [a, b], Martin Kružík [b, c, *]

[a] Charles University, Faculty of Mathematics and Physics, Sokolovská 83, 186 75 Prague, Czech Republic
[b] Czech Technical University, Faculty of Civil Engineering, Department of Physics, Thákurova 7, 166 29 Prague, Czech Republic
[c] Institute of Information Theory and Automation of the CAS, Pod Vodárenskou věží 4, 182 08 Prague, Czech Republic

ARTICLE INFO

Article history:
Received 1 September 2015
Received in revised form 28 December 2015
Available online 9 February 2016

Keywords:
B. Crystal plasticity
A. Microstructures
A. Deformation bands

ABSTRACT

Deformation bands are interpreted as a spontaneously formed microstructure caused by anisotropy induced by the slip nature of plastic deformation. The gradient terms in the proposed constitutive equations have been derived by averaging the assembly of discrete dislocations. The rigid-plastic model points to the main constituents which control the fragmentation mechanism: anisotropy of the hardening matrix, anisotropic resistance of the boundaries to slip, and the bowing (Orowan) stress. For symmetric double slip compression, the model provides an explanation of the observed band orientation and band width, and of the significant change in structural morphology seen as the band reorientation occurs at large strains. The predictions are in favorable agreement with available observations.

1. Introduction

In metal single crystals and polycrystals, a deformation microstructure evolves within a common framework. At all strain levels, the structural subdivision occurs in a form of elongated, alternately misoriented domains of a specific orientation. The domains, commonly called the *deformation bands*, are separated by roughly parallel families of geometrically necessary boundaries (GNBs). The deformation bands have only relatively recently come to light as a valuable tool for understanding the mechanism of plastic deformation (reviews, e.g. Bay et al., 1992; Kuhlmann-Wilsdorf, 1999; Hughes, 2001; Hansen and Jensen, 2011).

The inner structure built in the deformation bands depends on the character of slip, being different in cell forming and non-cell forming materials. In medium to high stacking fault energy crystalline materials at moderate strain (easy cross-slip, cell forming materials, e.g. rolled Al and Ni at von Mises effective strain $\bar{\varepsilon} \sim 0.3 - 0.7$), the deformation substructure most often consists of one or two sets of extended planar GNBs with a specific alignment, between which fairly equiaxed cells are formed (Bay et al., 1992; Hansen and Jensen, 2011; Hong et al., 2012). On the other hand, as observed by Hughes (1993), in the rolled Al–Mg, the framework for a crystal domain subdivision in non-cell forming metals is analogous to that observed in cell forming metals. However, the inner substructure of the deformation bands in Al–Mg consists of dislocations organized into a Taylor lattice containing multiple Burgers vectors. The domains have an alternating misorientation along the [111] slip plane. Unlike the rather sharp GNBs in the cell forming metals, the GNBs observed in the Al–Mg are diffuse.

* Corresponding author. Institute of Information Theory and Automation of the CAS, Pod Vodárenskou věží 4, 182 08 Prague, Czech Republic.
E-mail address: kruzik@utia.cas.cz (M. Kružík).

http://dx.doi.org/10.1016/j.ijplas.2016.01.016
0749-6419/

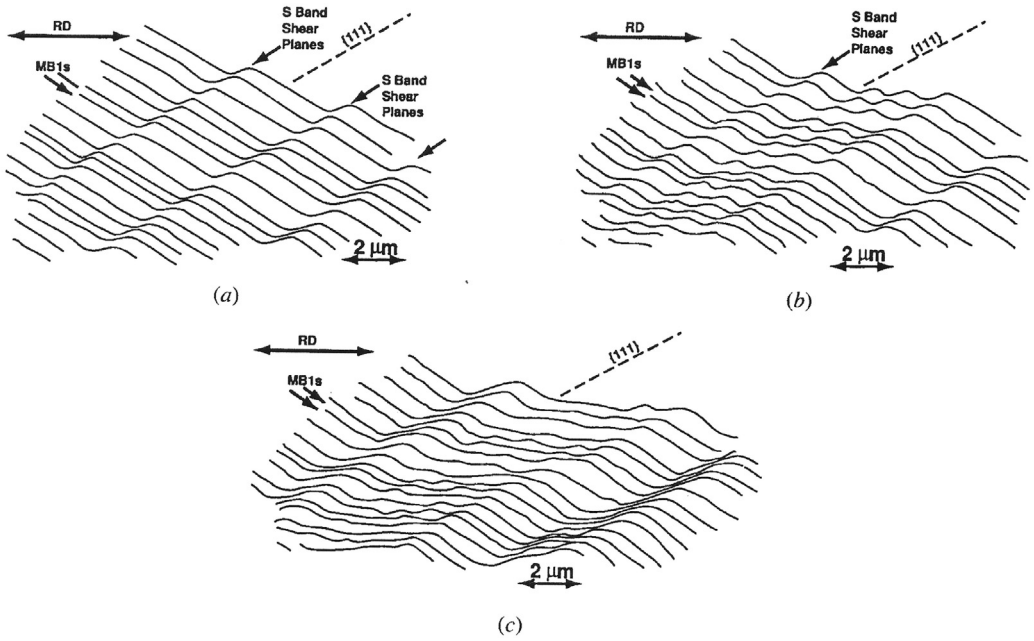

Fig. 1. Schema deduced from the micrographs of the transformation process of the large scale reorganization of the original MB and cell blocks microstructure to the lamellar structure oriented at a shallow angle to the RD (reproduced from Hughes and Hansen (1993)).

A typical microstructural evolution during rolling of fcc medium to high stacking fault energy metals has been analyzed in detail by Hughes and Hansen (1993, 2000). The deformation microstructures evolved in high purity nickel cold-rolled from 0.5 to 4.5 von Mises effective strain were observed and analyzed. Special focus was on factors which contribute to the transition from structures characteristic of small to medium strain microstructures to those characteristic of large strain microstructures (an analogous microstructure evolution was observed e.g. in Al and Al–Mg single crystals after room-temperature channel-die compression up to true strains 2.1 (Albou et al., 2010)). The observations reported in Hughes and Hansen (1993, 2000) can be summarized as follows.

To achieve energetically favorable strain accommodation, a subdivision occurs and created domains in which different slip systems operate. These domains have been defined as *cell blocks*. The cell blocks are bounded by GNBs which contain the lattice misorientation arising from as a consequence of strain accommodation. When increasing strain further exerted, the accommodation is met by refinement of the subdivision and by a change in substructural morphology.

At small strains, the GNBs bounding cell blocks are long single *dense dislocation walls* (DDWs) parallel to the transverse direction[1] and of a specific orientation with respect to the rolling direction (RD). With increasing strain, spacing between the DDWs decreases through the formation of new DDWs within the cell blocks, and misorientations across DDWs increase. The requirement of strain compatibility across the DDWs is met through further subdivision of the DDWs, which occurs by the formation of thin plate-like cell blocks in the DDWs. These new cell blocks have been defined as *microbands* (MBs). The DDWs and MBs have an orientation to the RD with no crystallographic preference.

At intermediate strain, most of the cell blocks are delineated by MBs which have formed from DDWs. These MBs have a characteristic morphology composed of parallel dislocation walls or small pancake-like cells, and the thickness of the MBs ranges from 0.1 to 0.4 μm. There are cells both within and between the MBs. Since MBs are formed from the DDWs, they maintain the same orientation with respect to the RD. Two families of the MBs have been observed: one being oriented $\pm 30^\circ$ to the RD and the other inclined $\pm 15^\circ$ to the RD. There is a difference for rolled nickel and aluminum: for aluminum, the peak in the distribution of orientations for the first family of MBs remains at 40° to the RD, whereas for nickel this peak shifts to 30° with increasing strain (Hughes and Hansen, 1993).

At intermediate strain, in addition to the MBs and DDWs, there have been observed dislocation configurations in which localized shear along {111} planes can develop. The most prominent are the bands of intense local crystallographic slip which intersects parallel groups of MBs, and thus creates a string of "S" shaped perturbations in the pre-existing MB structure. The *bands of the intense local slip* (called in Hughes and Hansen (1993) *S-bands*)[2] are narrow, from 0.05 to 0.3 μm in thickness, and long, with length ranging from 5 to 20 μm. Nearly all of the shear planes of these bands are parallel to a {111} slip plane within

[1] The transverse direction is in the rolling plane perpendicular to the rolling direction. The lateral (longitudinal) plane is parallel to the rolling direction and to the normal direction of the rolling plane.

[2] Note that the perturbed MBs become S-shaped, while the S-bands are straight.

5°. The intersecting S-bands tilt locally short sections of several MB walls leaving a string of S-shaped configurations. These S-shaped configurations have been observed over a wide strain range, from 0.5 to 3.5 effective strain.

The passage of regularly distributed S-bands causes a large scale reorganization of the original MB and cell blocks microstructure to a lamellar structure oriented at shallow angles to the RD (schematic drawings of the transformation process are shown in Fig. 1, reproduced from Hughes and Hansen (1993)). Initially, there is a wide spacing of S-bands. As deformation continues, new S-bands are formed between the previous S-bands. A family of S-bands forms in an evenly distributed manner at an angle to the original MBs; according to the schematic drawings in Fig. 1, the families of MBs and S-bands are oriented nearly symmetrically with respect to the normal direction (the direction perpendicular to the rolling plane). The shear within S-bands causes local tilting of MB walls resulting in a sharply stepped wall configuration. There is a further tendency for the stepped MB walls to straighten in order to decrease their length and thereby their energy. As the stepped walls straighten, there is a net realignment of the walls closer to the RD. The formed *lamellar boundaries* (LBs) are distinguished from the MBs by both their orientation closer to the RD and their larger misorientations. The lamellar boundaries are frequently layered closely together with narrow cells between them, and together form very thin cell blocks. In adjacent areas, these boundaries also sandwich layers of equiaxed and slightly elongated subgrains. The transition from a microstructure composed of MBs and DDWs to one composed of LBs occurs gradually over a very large strain range from an effective strain of 0.5–3. At the very high effective strain of 4.5, no remaining MBs have been observed, and the structure is dominated by the LBs almost parallel to the RD. The narrow channels between the LBs are bridged by interconnected cell boundaries which are approximately perpendicular to the RD and form a bamboo structure. The family of MBs oriented $\pm 15^\circ$ to RD seems to transform to the lamellar structure directly without any help of S-bands.

A comprehensive review of continuum mechanic approaches to the deformation banding has been given by Petryk and Kursa (2013). A constitutive framework for elastic–plastic finite deformation has been formulated by Hill (1966) and Hill and Rice (1972) widely applied namely in study of formation of shear bands e.g. (Asaro, 1979, 1983; Peirce et al., 1983; Bassani, 1994). The shear bands arise from a material softening (including geometrical softening (Asaro, 1983)). On the other hand, the deformation bands result from hardening anisotropy: it is energetically less costly to flow the material through the crystal lattice buckled by the deformation bands with a decreased number of active slip systems than to flow it through a lattice homogeneously deformed by multi slip.

The model of deformation banding developed by Ortiz and Repetto (1999), Ortiz et al. (2000) is based on incremental minimization of the pseudo-elastic energy. They assumed that the corresponding energy densities undergoing latent hardening are non-convex with energy preference for single slip. Such incremental energy potential exists locally if the deformation field is split into compatible domains of single slip on different slip systems. In computations, such splitting was enforced by assuming infinite latent hardening (Aubry and Ortiz, 2003). The model has been applied in a simulation of a microstructure evolution in an equal channel angular extrusion process (Sivakumar and Ortiz, 2004). The specific structures considered in the simulations were of the sequential lamination type.

Within the small-deformation framework, Gurtin and Reddy (2014) have introduced a rate-independent gradient single crystal plasticity which accounts for self and latent hardening. A large-strain viscoplastic extension simulated by the model presented in Bargmann et al. (2014) has been employed in a computational investigation of the model of the interactive slip resistance. Computational studies comparing gradient-enhanced plasticity with relaxation approaches to nonconvex problems were performed in Klusemann and Kochmann (2014), Klusemann and Yalinkaya (2013). The used relaxation ansatz assumes presence of shear bands in the form of the so-called first order laminates. Comparison with experiments reported in Klusemann and Kochmann (2014) drew a conclusion that gradient plasticity models are more realistic than the standard approach.

From the rich theoretical literature on crystal deformation banding (a brief survey of the models is given e.g. in Arul Kumar and Mahesh (2012)), one of the most relevant models to the approach presented here is the model proposed by Mahesh (2006, 2012, 2015) and Arul Kumar and Mahesh (2012, 2013). Crystal is regarded as an one-dimensional stack of parallelepiped-shaped domains that collectively accommodate the imposed deformation. Each domain, modeling a band, deforms homogeneously and compatibly with their neighbors. The suggested model is based on three hypotheses that determine the preferred band boundary orientation in the rigid-plastic model of an arbitrarily oriented crystal: (i) a uniform state of stress prevails throughout the crystal; (ii) the bands are disoriented so as to minimize the power of plastic deformation; and (iii) their boundaries are oriented so as to minimize plastic incompatibility between the neighboring domains. The model presented in Arul Kumar and Mahesh (2012) simulated plane strain compression of copper single crystals. The model predicted the formation of shear bands and deformation bands in the crystals of the initial copper and cube orientation, and the formation of neither of them in the Gross oriented single crystal. The predicted orientations and disorientations have compared favorably with those reported in experimental literature. The solution in the form of a stream function which can be interpreted as a deformation band-like pattern in the present paper, Section 2, is akin to the stack of the domains. However, in Mahesh et al. approach, the cell block predictions are independent of latent hardening of slip systems. On the other hand, a strong latent hardening plays a key role in the present and e.g. in Aubry and Ortiz (2003) modeling of the deformation bands.

Let us note that an interesting and original approach has been proposed by Winther (2012), Winther et al. (2014). She calculated the dislocation configuration in GNBs and its misorientation by means of the low energy dislocation structures (LEDS) principle, and by assuming the boundaries free of long range stresses. Following Leffers (2001a, 2001b), the

misorientations across the boundaries were evaluated using a continuum mechanics condition that the neighboring cell blocks with different slip system activities must remain in contact at the boundaries.

In a currently most advanced theoretical investigations, Petryk (1992, 2000), Petryk and Thermann (2002), Petryk and Kursa (2011, 2013) aimed to clarify a formulation and a justification of the incremental energy criterion for deformation banding in crystals locally deformed by multi slip. In the criterion for incipient deformation banding, the key role is played by symmetrization of the hardening submatrix restricted to the active slip systems in the energy minimization solution. Additionally, the second order minimization has been extended to a finite time step in order to enable numerical calculations of the initial modes of deformation banding, and tracing deformation paths under external control. In view of that, an attempt has been made to simulate the deformation band pattern under tension with the focus on predicting three distinct microstructure types observed experimentally in three different domains of the tensile axis orientation (Huang and Winther, 2007; Winther and Huang, 2007). No length scale effect has been studied. The simplified model introduced in the next Sections presents the essence of the energetic approach of Petryk–Kursa's type.

In the present paper, the modeling of the observed properties of the deformation bands, summarized in the first part of this Section, is based on the mechanics of incremental deformations proposed by Biot (1965). He was probably the first one who treated deformation bands (which he called the instability of the first kind) as a consequence of material anisotropy. Biot's theory provides rigorous and completely general equations governing the dynamics and stability of solids and fluids under initial stress in the context of small perturbations. The method allows for using the linear theory of incremental deformations even for the analysis of advance stages of deformation. The main idea of this method is to expose a given homogeneous or homogenized deformation state to an incremental, generally inhomogeneous deformation mode and to evaluate the incremental work needed to carry out the deformation. The lowest incremental work indicates a tendency to a change and points to the preferred mode which will dominate the evolving deformation substructure.

We employ Biot's theory of instability modes to reveal mechanisms responsible for deformation banding and their observed features. We use the original Biot's model (Biot, 1965), which is modified for crystal plasticity and enriched with a dislocation boundary resistance to slip and length scale effect. We apply the Biot's model of orthotropic materials where the orthrotropy is carried by symmetric double slip with distinguished latent hardening. The orthotropy guarantees the symmetry of the hardening matrix, which enables a variational formulation and the energy minimization process. The plane strain model has already been employed by Harren et al. (1988) and in our previous publications (Kratochvíl and Orlová, 1990; Kratochvíl, 1990; Kratochvíl et al., 2009). In Harren et al. simulations of a plane strain compression of the (110)[001] geometry (Harren et al., 1988), the four observed active slip systems of the directions $[10\overline{1}]/2$ and $[01\overline{1}]/2$ in the (111) plane and of the directions [101]/2 and [011]/2 in the $(11\overline{1})$ plane are approximated by a two-dimensional single crystal model with two effective slip systems $(111)[11\overline{2}]$ and $(11\overline{1})[112]$. The orientation of the slip systems with respect to the compression axis is $\phi = 35^\circ$. The GNDs corresponding to the effective slip systems are reduced to edge dislocations parallel to the transverse direction. The properties of glide dislocations (e.g. in a form of dislocation loops with screw parts exposed to cross-slip), which carry plastic deformation and build up the GNBs, enter the model implicitly through hardening coefficients. Here, we use mainly the papers (Sedláček and Kratochvíl, 2005; Kratochvíl and Sedláček, 2004; Kratochvíl et al., 2007) recalled in the next Section as a starting point for our considerations.

In the next Section, a symmetric double slip model of a spontaneous formation of the deformation bands is presented. We adopt the rigid-plastic, rate-independent approximation, which turns out to be the optimal viewpoint pointing to the essential features of the formation of the deformation bands. We follow the classical crystal plasticity framework except for a modification of the hardening rule (Equation (14)). The modified rule incorporates a hardening caused by the incremental work needed to overcome the resistance to buildup the geometrically necessary boundaries and to overcome the dislocation bowing stress. The proposed rule has been motivated by statistical considerations (Kratochvíl et al., 2007) based on averaging of an assembly of discrete dislocations. A variational form suitable for energetic consideration is presented in Section 3. For the special case of symmetric double slip compression, the results of Section 4 provide an interpretation of the band orientation, their width, and the significant change in the structural morphology seen as the band reorientation occurring at large strains. A preliminary version of the model has been outlined in Kratochvíl and Kružík (2014).

2. Model of deformation bands

We consider a plane-strain compression of an infinitely extended rigid-plastic crystal domain in the coordinate system (x, y), Fig. 2, with the symmetry axis coinciding with the y coordinate axis. The angle of the slip planes with respect to the y axis is $\phi = 35^\circ$. The plane strain compression simulating a cold-rolling process is assumed to be homogeneous (or homogenized) up to a certain deformation level. The deformation increment at this point can be either homogeneous again, or else, it can be inhomogeneous. The aim of the analysis is to determine the conditions under which the deforming crystal domain prefers an inhomogeneous increment in a form of deformation bands.

The incremental deformation representing a deviation from the original symmetric double slip is expressed through an incremental displacement vector $\boldsymbol{u}(x, y)$. The displacement gradient $\nabla \boldsymbol{u}$ can be decomposed into a plastic part, which represents the material flow carried by dislocations, and an elastic part. In the rigid-plastic approximation the elastic part reduces to an increment of the rigid rotation of the crystal lattice $\boldsymbol{\omega}^*$. For small increments, the decomposition reads $\nabla \boldsymbol{u} = \boldsymbol{\beta} + \boldsymbol{\omega}^*$, where β is the increment of the plastic distortion caused by incremental slips $\gamma^{(1)}(x, y)$ and $\gamma^{(2)}(x, y)$ on the two considered slip systems, Fig. 2. This relation can be expressed as

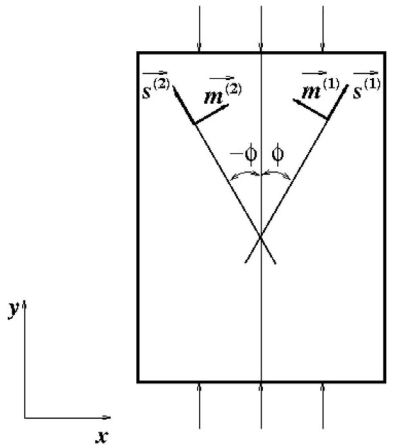

Fig. 2. Symmetric double slip in plane strain compression.

$$\beta = \sum_{i=1}^{2} \gamma^{(i)} s^{(i)} \otimes m^{(i)}, \tag{1}$$

$s^{(1)} = (\sin\phi, \cos\phi)$ and $\boldsymbol{s}^{(2)} = (-\sin\phi, \cos\phi)$ represent the slip directions, and $\boldsymbol{m}^{(1)} = (-\cos\phi, \sin\phi)$ and $\boldsymbol{m}^{(2)} = (\cos\phi, \sin\phi)$ are the unit slip plane normals; $\pm\phi$ is the orientation angle of the slip planes with respect to the symmetry axis of the compression.

The incremental strain $\boldsymbol{\varepsilon}(x, y)$ superposed upon the current homogeneous (or homogenized) strain $\bar{\boldsymbol{\varepsilon}}$ is defined as $\boldsymbol{\varepsilon} = (\nabla \boldsymbol{u} + (\nabla \boldsymbol{u})^{\boldsymbol{T}})/2$. For the model considered, one can deduce from (1)

$$\varepsilon_{xx} = -\varepsilon_{yy} = -\sin 2\,\phi\left(\gamma^{(1)} + \gamma^{(2)}\right)\Big/2, \quad \varepsilon_{xy} = -\cos 2\,\phi\left(\gamma^{(1)} - \gamma^{(2)}\right)\Big/2. \tag{2}$$

The increments of the lattice rotation ω^*, representing an increment of the lattice misorientation, is related to the increments of the material rotation $\omega = \omega_{xy} = (\partial_y u_x - \partial_x u_y)/2$ and an increment of the plastic rotation $\omega^p = (\gamma^{(1)} - \gamma^{(2)})/2$ as $\omega^* = \omega - \omega^p$. In general, the elastic and plastic parts of the incremental deformation $\nabla \boldsymbol{u}$ may be individually incompatible. The incremental density of the geometrically necessary dislocations (GNDs), superposed on the current homogenized GND structure, required for the deformation to remain compatible is characterized by the increment of the dislocation density tensor $\boldsymbol{\alpha} = \operatorname{curl} \boldsymbol{\beta} = -\operatorname{curl} \boldsymbol{\omega}^*$. This relation reveals the relation between the incremental slips and the increment of the density of GNDs expressed[3] by the tensor $\boldsymbol{\alpha}$. Within the approximation employed in this paper, the increment α indicates a trend in the GND structure evolution.

The tensor α can be resolved in the incremental densities $\boldsymbol{\alpha}^{(i)}$, $i = 1, 2$, of GNDs of the individual slip systems,

$$\alpha = \alpha^{(1)} + \alpha^{(2)} = \sum_{i=1}^{2} curl\, \beta^{(i)} = \sum_{i=1}^{2} curl\left(\gamma^{(i)} s^{(i)} \otimes m^{(i)}\right). \tag{3}$$

The tensors $\boldsymbol{\alpha}^{(i)}$ specify the incremental effective edge dislocation composition of the geometrically necessary boundaries (GNBs) in the plane strain approximation suggested by Harren et al. (1988). In this approximation, the density increments are reduced to the single non-zero components

$$\alpha^{(1)} = \left(\sin\phi\,\partial_x + \cos\phi\,\partial_y\right)\gamma^{(1)}, \quad \alpha^{(2)} = \left(-\sin\phi\,\partial_x + \cos\phi\,\partial_y\right)\gamma^{(2)}. \tag{4}$$

As for boundary conditions, we consider an infinitely extended solid and assume periodicity in x and y directions of all the incremental fields. For instance,

[3] In the framework of large deformations (Sedláček, 1999; Cermelli and Gurtin, 2001), the increment α consists of two contributions: the increment caused by the change of the crystal lattice orientation and the increment due to the slip increments. In the small strain approximation, only the latter contribution is retained.

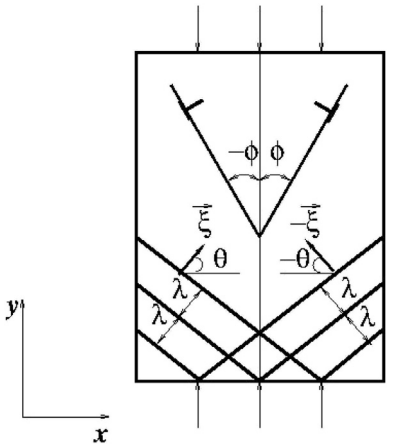

Fig. 3. Schema of two sets of deformation bands perpendicular to the vectors $\pm\xi$, λ is the band width.

$$\varepsilon(x,y) = \varepsilon\big(x + L_x, y + L_y\big), \tag{5}$$

where L_x and L_y are the lengths of one period in the corresponding directions. Since the lengths L_x and L_y can be extended to infinity, the periodicity is only a formal requirement. It enables us to omit the boundary terms that would otherwise appear when applying Green's theorem in the integral formulation in Section 3.

To satisfy the incompressibility of the increment of the deformation $\varepsilon_{xx} + \varepsilon_{yy} = \partial_x u_x + \partial_y u_y = 0$, we make use of the stream function ψ so that $u_x = \partial_y \psi, \quad u_y = -\partial_x \psi$. We look for an inhomogeneous, kinematically admissible increment of the deformation, which can be constructed from the stream function ψ in the form

$$\psi = F(x + \xi y), \tag{6}$$

which represents an inhomogeneous increment of simple shear parallel to the planes $x + \xi y =$ constant. The shear inhomogeneity can be interpreted as a deformation band-like pattern perpendicular to the direction $\xi = \tan\theta$, where θ is the angle between the x axis and the normal to the bands, Fig. 3. In view of the linearity of the problem at hand, any linear combination of the stream functions of the type (6) with different profiles F and directions ξ is kinematically admissible. The kinematically admissible strains and rotations are derived by means of the stream function ψ and the kinematic relations $\boldsymbol{\varepsilon} = (\nabla \boldsymbol{u} + (\nabla \boldsymbol{u})^{\boldsymbol{T}})/2$ and $\boldsymbol{\omega} = (\nabla \boldsymbol{u} - (\nabla \boldsymbol{u})^{\boldsymbol{T}})/2$

$$\varepsilon_{xx} = \xi F'', \quad \varepsilon_{xy} = \frac{1}{2}\left(\xi^2 - 1\right)F'', \quad \omega \equiv \omega_{xy} = \frac{1}{2}\left(\xi^2 + 1\right)F'', \tag{7}$$

where F'' represents the second derivative of F with respect to the argument $x + \xi y$. Kinematically admissible crystallographic slip increments then result from (2),

$$\gamma^{(1)} = \left(\frac{1-\xi^2}{2\cos 2\,\phi} - \frac{\xi}{\sin 2\,\phi}\right)F'', \quad \gamma^{(2)} = \left(\frac{\xi^2-1}{2\cos 2\,\phi} - \frac{\xi}{\sin 2\,\phi}\right)F'', \tag{8}$$

and using (4) we obtain for the increments of the dislocation densities

$$\begin{aligned} \alpha^{(1)} &= (\sin\phi + \xi\cos\phi)\left(\frac{1-\xi^2}{2\cos 2\phi} - \frac{\xi}{\sin 2\phi}\right)F'', \\ \alpha^{(2)} &= (-\sin\phi + \xi\cos\phi)\left(\frac{\xi^2-1}{2\cos 2\phi} - \frac{\xi}{\sin 2\phi}\right)F''. \end{aligned} \tag{9}$$

The increment of the alternating lattice misorientation ω^* and the incremental plastic rotation ω^p are expressed as

$$\omega^* = \frac{\left(\xi^2+1\right)\cos 2\phi + \xi^2 - 1}{2\cos 2\phi}F'', \quad \omega^p = \left(\gamma^{(1)} - \gamma^{(2)}\right)\big/2 = \left(\frac{1-\xi^2}{2\cos 2\phi}\right)F''. \tag{10}$$

The stress $\boldsymbol{\sigma_R}$ in the deforming crystal domain, expressed in a reference frame which rotates with the crystal lattice, consists of three contributions

$$\boldsymbol{\sigma_R} = \overline{\boldsymbol{\sigma}} + \boldsymbol{\sigma} + \boldsymbol{\omega^p}\overline{\boldsymbol{\sigma}} + \overline{\boldsymbol{\sigma}}(\boldsymbol{\omega^p})^{\mathrm{T}}. \tag{11}$$

$\overline{\boldsymbol{\sigma}}$ is the applied homogeneous stress which in a given state of the plastic regime has a character of a pre-stress. In the considered case of the plane strain compression, the stress $\overline{\boldsymbol{\sigma}}$ has a single component, $\overline{\sigma}<0$, in the y direction as shown in Fig. 3. σ is the stress increment and the term $\boldsymbol{\omega^p}\overline{\boldsymbol{\sigma}} + \overline{\boldsymbol{\sigma}}(\boldsymbol{\omega^p})^{\mathrm{T}}$ accounts for the geometrical hardening/softening, i.e. for a change in the stress due to the rotation of the pre-stress tensor with respect to the crystal lattice (a justification is e.g. Biot, 1965).

The corresponding stress equilibrium is

$$\begin{aligned} &\partial_x\sigma_{xx} + \partial_y\sigma_{xy} + \overline{\sigma}\partial_y\omega = 0,\\ &\partial_x\sigma_{xy} + \partial_y\sigma_{yy} + \overline{\sigma}\partial_x\omega = 0. \end{aligned} \tag{12}$$

The slip increments are induced by the increments in the resolved shear stresses $\tau^{(i)} = \boldsymbol{s}^{(i)}\cdot\boldsymbol{\sigma}\,\boldsymbol{m}^{(i)}$, $i = 1, 2$, which results in

$$\tau^{(1)} = -\sin 2\,\phi\big(\sigma_{xx} - \sigma_{yy}\big)/2 - \cos 2\,\phi\;\sigma_{xy}, \quad \tau^{(2)} = -\sin 2\,\phi\big(\sigma_{xx} - \sigma_{yy}\big)/2 + \cos 2\,\phi\;\sigma_{xy}. \tag{13}$$

In the rate-independent approximation the resolved shear stress increment in the plastic regime equals the flow stress increment. This is accounted for by the hardening rule which plays a central role in the proposed model. To describe the deformation band orientation and the band width, the standard crystal plasticity hardening rule has to be enriched with additional features. The boundaries of the deformation bands consist of geometrically necessary dislocations (GNDs). Building up the boundaries requires additional work to overcome their resistance to slip. Moreover, the shrinking width of the bands decreases the space for the dislocation glide, hence their bowing stress grows and causes a line tension (Orowan) strengthening. These effects can be incorporated in the model by a modification of the standard hardening rule[4]

$$\begin{aligned} \tau^{(1)} &= (h + h_{bow})\,\gamma^{(1)} + qh\,\gamma^{(2)} + \tilde{h}\,\boldsymbol{s}^{(1)}\cdot\nabla\alpha^{(1)} + \tilde{q}\tilde{h}\,\boldsymbol{s}^{(1)}\cdot\nabla\alpha^{(2)},\\ \tau^{(2)} &= qh\,\gamma^{(1)} + (h + h_{bow})\gamma^{(2)} + \tilde{q}\tilde{h}\,\boldsymbol{s}^{(2)}\cdot\nabla\alpha^{(1)} + \tilde{h}\,\boldsymbol{s}^{(2)}\cdot\nabla\alpha^{(2)}. \end{aligned} \tag{14}$$

The entries are the self-hardening coefficient h and the latent (cross) hardening coefficient qh. The latent-to-active hardening ration q is a measure of the hardening anisotropy, being one of the key parameters of the model. The gradient terms in (14) led by $\tilde{h}$ and $\tilde{q}\tilde{h}$ have been derived by averaging the assembly of discrete parallel edge dislocations at plane strain conditions in Kratochvíl et al. (2007). The coefficient h_{bow} controls the bowing stress.

In general, work hardening is governed by short-range interactions between dislocations: (i) by self-force of the curved dislocations, and (ii) by forces depending on short-range correlations between dislocations.

(i) Within the framework of a 3D statistical model of curved dislocations (Kratochvíl and Sedláček, 2008), the self-force has been expressed in the line tension approximation where the higher gradient is introduced automatically through a dislocation curvature. Here, we employ a standard form of the line tension strengthening $h_{bow} = 2\sin\beta_c\, Gb/d$, where the critical angle β_c characterizes the penetrability of obstacles and d is the distance between obstacles causing the dislocation bowing; $1/d$ approximates the curvature. G is the shear modulus and b the magnitude of the Burgers vector. In the present context, the prominent obstacles are most probably the cell boundaries formed within the deformation bands. The cell size changes in a monotonic way with the changing width of the bands. Therefore, the distance d is identified with the band width λ. In the present, model we assume a partial penetrability of the boundaries assuming that $h_{bow} = Gb/\lambda$. The hardening term h_{bow} is added to the self hardening part of the standard rule (14). The reason is that the dislocation bowing hinders the active slip, but causes no additional latent hardening.

(ii) The short-range correlation forces are non-local and they should be expressed in an integral form. The result (14) of the statistical considerations (Kratochvíl et al., 2007) has been restricted to the model of parallel edge dislocations (the reason is that a statistical treatment of curved dislocations is far less straightforward, mainly because it has to be accounted for the connectivity of dislocations (Kratochvíl and Sedláček, 2008)). In (14), only two types of the interaction terms of the expansion of the short-range correlation integrals have been retained. The terms in (14) led by h and qh represent the standard local hardening which depends on the so-called statistically distributed dislocations. Their density increases with increasing slip increments $\gamma^{(1)}$ and $\gamma^{(2)}$. On the other hand, the terms led by $\tilde{h}$ and $\tilde{q}\tilde{h}$ express

[4] In an alternative constitutive equations analyzed in Kratochvíl and Kružík (2015), the boundaries have been treated as interfaces. The critical resolved shear stress has been split into a bulk part identical to the terms in (14) led by $h + h_{bow}$ and by hq, and the boundary part. In the boundary part, the GNBs are treated as planar interfaces suitable for modeling of the sharp GNBs in cell forming metals. The GNBs have been characterized by a matrix of the boundary part of the flow rule in an analogy to the bulk anisotropic hardening. The quantification of the coefficients controlling the boundary part has encountered the same problem as $\tilde{h}$ and $\tilde{q}$, and the coefficients have been employed as fitting parameters. At present, we cannot determine whether the gradient model presented here or the interface model (Kratochvíl and Kružík (2015)) is closer to reality. Nevertheless, both models underline the importance of the boundary anisotropic properties in deformation banding.

that the resistance to the dislocation motion depends also on the arrangement of the dislocations. The gradients of the increments of the GND densities $\alpha^{(i)}$, $i = 1, 2$, are taken as simplified characteristics of that arrangement. In the present context, the gradient terms in (14) can be interpreted as the resolved shear stress increments needed to penetrate a cluster of the GNDs of the same ($\tilde{h}$) or the other slip system ($\tilde{q}\tilde{h}$). The length scale contained in $\tilde{h}$ and $\tilde{q}\tilde{h}$ can be understood as an effective radius of the non-local interaction.

The problem of an adequate specification and evaluation of the short-range correlations between dislocations represents the main challenge when trying to quantify the proposed model. There is a number of microstructural mechanisms which control the interactions between dislocations and the boundaries. In general, the interaction depends on the slip system orientation, the relative misorientation across the boundaries, and the net accumulated slip at the boundaries. The boundary resistance to slip could incorporate a strength of dislocation nucleation close to the boundaries, and might involve the additional work required to overcome the configurational changes necessary for a dislocation to enter the boundary. Such changes might include the recombination or dissociation of partial dislocations, which depends on the stacking fault energy. Existing approaches to these problems and encountering difficulties have been reviewed in van Beers et al., 2013).

In the attempt based on the statistical considerations presented in Kratochvíl et al. (2007), the coefficient $\tilde{h}$ has been estimated as

$$\tilde{h} \approx \frac{G}{2\pi(1-\nu)} \frac{D}{\delta\rho}, \tag{15}$$

where ρ is the dislocation density in the GNBs, δ represents the GNB width, and the factor D expresses an average geometry of the correlation among dislocations. From the comparison of the statistical model with the illustrative single slip example of dynamics of the discrete parallel edge dislocations (Groma et al., 2003), it has been deduced that $D = 0.8$. For $G = 7 \times 10^{10}$Pa, $\nu = 0.3$, $\rho = 10^{15}\mathrm{m}^{-2}$, and $\delta = 10^{-9}$m relation (15) gives the estimate $\tilde{h} = 15 \times 10^{3}$Pa , m = 15MPa μm. Due to the severely simplified assumptions involved in the estimate of $\tilde{h}$, its validity is highly non-reliable.

Estimates of the coefficients $\tilde{h}$ and $\tilde{q}$ based on discrete dislocation dynamics could be more successful and useful in the future. However, as indicated in the present paper, GNBs arise due to the laws of continuum mechanics. Therefore, an evaluation of the coefficient would require a framework of discrete dislocation dynamics combined with continuum mechanics. As demonstrated e.g. in Vattre et al. (2014), a formulation of a continuous-discrete model is still a challenging problem.

The current practice is to use the boundary resistance coefficients $\tilde{h}$ and $\tilde{q}$ as fitting parameters. A recent attempt to quantify the grain boundary interface mechanisms in the framework of strain gradient plasticity has been presented in van Beers et al. (2013). The proposed grain boundary model incorporates the boundary slip resistance and the boundary free energy parameter, both taken as material constants. The influence of these parameters on plastic deformation of a numerical model of a bicrystal has been investigated for shear strain up to 0.1%. The range of the slip resistance used in the test has been 0.03–0.15 N/mm, i.e. 30–150 MPa μm. The influence of the boundary free energy coefficient has been tested in the interval $0–10^{6}$. For these values, a qualitative agreement between the model prediction and the available experimental observations has been achieved. As noted in van Beers et al. (2013), a quantitative calibration and validation of the proposed model of the grain boundary interface mechanisms is hindered by a lack of suitable experimental data. In the modeling of the combined effect of a grain size and a grain shape on macroscopic plastic anisotropy, the authors Delannay and Barnett (2012) introduced a material constant B accompanying the gradient term similarly as $\tilde{h}$ in (14). The constant B enters a reference length together with the amplitude of the slip gradient at the boundary, taken as another constant. In the computation, the reference length was set to be the average value of the shorter grain radius of the considered columnar grains.

In the described situation we have not found any reliable guideline for an estimate of the slip resistance coefficients $\tilde{h}$ and $\tilde{q}$. Therefore, they enter the proposed model, similarly as in van Beers et al. (2013), Delannay and Barnett (2012), as fitting parameters. Nevertheless, one of the main results is that the paper points to a possibility that the slip resistance of GNBs and its anisotropy, i.e. the resistance to the different slip systems does not need to be the same, might be a key factor controlling the deformation band substructure evolution.

Note that keeping only the self-hardening coefficient h and the latent (cross) hardening coefficient qh in the hardening rule (14), the Equations (2), (13) and (14) lead to the incremental constitutive relations for an orthotropic, incrementally-linear rigid-plastic solid in the form proposed by Biot (1965), namely

$$\sigma_{xx} - \sigma_{yy} = 2H_{xx}(\varepsilon_{xx} - \varepsilon_{yy}), \quad \sigma_{xy} = 2H_{xy}\varepsilon_{xy}, \tag{16}$$

where the instantaneous hardening coefficients are

$$H_{xx} = \frac{h(1+q)}{2\sin^2 2\phi}, \quad H_{xy} = \frac{h(1-q) + \overline{\sigma}\cos 2\phi}{2\cos^2 2\phi}. \tag{17}$$

As demonstrated by Biot (1965) and recalled in Sedláček and Kratochvíl (2005), Kratochvíl and Kruzik (2014), Biot's orthotropic model provides the basic result of the energetic approach – *the existence of the deformation bands*. It was shown,

however, that the predicted bands have extremal properties: the band orientation is perpendicular to the direction of the compression (i.e. parallel to rolling direction) and their width tends to approach zero.

3. Energetic formulation

For the purpose of the energy considerations, the problem is cast in terms of a variational formulation. We employ the principle of virtual displacements, hence from stress equilibrium (12)

$$\int_{\Omega} \left(\left(\partial_x \sigma_{xx} + \partial_y \sigma_{xy} + \overline{\sigma} \partial_y \omega \right) \delta u_x + \left(\partial_x \sigma_{xy} + \partial_y \sigma_{yy} + \overline{\sigma} \partial_x \omega \right) \delta u_y \right) \mathrm{d}V = 0, \tag{18}$$

where Ω is the crystal domain in the xy plane and $\delta \boldsymbol{u}(x,y)$ is an arbitrary virtual displacement field. Using Green's theorem and the chosen periodic boundary conditions, we obtain the weak form of the equilibrium Equation (12)

$$\int_{\Omega} \left(\sigma_{xx} \delta \varepsilon_{xx} + 2 \left(\sigma_{xy} + \overline{\sigma} \omega \right) \delta \varepsilon_{xy} + \sigma_{yy} \delta \varepsilon_{yy} \right) \mathrm{d}V = 0. \tag{19}$$

The weak formulation is equivalent to the requirement that the energy functional J attains a minimum. A condition for this is that the first variation of the functional J equals zero:

$$\delta J = 0. \tag{20}$$

From this condition using (2), (13) and (14), the functional J can be evaluated in the form

$$J = 2 \int_{\Omega} \left\{ (h + h_{bow}) \left[\left(\gamma^{(1)} \right)^2 + \left(\gamma^{(2)} \right)^2 \right] + 2qh\, \gamma^{(1)} \gamma^{(2)} + \frac{\overline{\sigma} \cos 2\phi}{2} \left(\gamma^{(1)} - \gamma^{(2)} \right) \left(\gamma^{(1)} - \gamma^{(2)} + \omega \right) - \tilde{h} \left[\left(\boldsymbol{s}^{(1)} \cdot \nabla \gamma^{(1)} \right)^2 + \left(\boldsymbol{s}^{(2)} \cdot \nabla \gamma^{(2)} \right)^2 \right] - 2 \tilde{q} \tilde{h} \left(\boldsymbol{s}^{(1)} \cdot \nabla \gamma^{(1)} \right) \left(\boldsymbol{s}^{(2)} \cdot \nabla \gamma^{(2)} \right) \right\} dV. \tag{21}$$

Introducing the stream function (6) using relations (8) and $(7)_3$ evaluated for the considered microstructure ξ of Fig. 3, the functional (21) becomes.

$$J = \frac{1}{2} \left(4 [H_{xx} + B_{xx}] \xi^2 + [H_{xy} + B_{xy}] \left(\xi^2 - 1 \right)^2 - \frac{\overline{\sigma}}{2} \left(1 - \xi^4 \right) \right) \int_{\Omega} \left(F'' \right)^2 \mathrm{d}V - \frac{1}{2} \left(K_1 \xi^4 + K_2 \left(1 - \xi^2 \right)^2 + L_1 \xi^2 + L_2 \xi^2 \left(1 - \xi^2 \right)^2 + M \xi^2 \left(\xi^2 - 1 \right) \right) \int_{\Omega} \left(F''' \right)^2 \mathrm{d}V, \tag{22}$$

where H_{xx} and H_{xy} are given by (17) and

$$K_1 = \frac{\tilde{h}(1+\tilde{q})}{2 \sin^2 \phi}, \quad K_2 = \frac{\tilde{h}(1+\tilde{q}) \sin^2 \phi}{2 \cos^2 2\phi}, \quad L_1 = \frac{\tilde{h}(1-\tilde{q})}{2 \cos^2 \phi}, \quad L_2 = \frac{\tilde{h}(1-\tilde{q}) \cos^2 \phi}{2 \cos^2 2\phi}, \tag{23}$$

$$B_{xx} = \frac{h_{bow}}{2 \sin^2 2\phi}, \quad B_{xy} = \frac{h_{bow}}{2 \cos^2 2\phi}, \quad M = \frac{2\tilde{h}}{\cos 2\phi}. \tag{24}$$

To see which inhomogeneous incremental deformation is energetically favorable, the inhomogeneous incremental stain represented by the profile $F''(x+\xi y) \neq 0$ is assumed to be such a deviation from a homogeneous increment, that the average of the corresponding strains equals zero. A homogeneous increment can be formally represented by $F''(x+\xi y) = 0$. Thus, the functional (22) now represents an energy difference between the homogeneous and inhomogeneous deformation increments. The inhomogeneous deformation increment is energetically favorable if the functional (22) becomes negative, $J < 0$. If a kinematically possible deformation exists that fulfills this condition, then the homogeneous deformation is unstable and a pattern is formed.

To analyze a particular pattern, we consider the deformation banding inspired by a band substructure observed in the cell forming metals, i.e. the periodically arranged homogeneously sheared deformation bands perpendicular to the direction ξ separated by the sharp geometrically necessary boundaries (GNBs). The shear strain alternates: $F'' = \pm(a/\lambda)$, where a is an amplitude of the incremental displacement and λ is the width of the bands.[5] The total area of GNBs in the crystal domain Ω of

[5] The functional (22) with the smooth profile F'' could be suitable for simulation of diffuse GNBs, as observed in non-cell forming metals (Hughes, 1993).

Table 1
Model parameters of the cell block structure at moderate strains $\bar{\varepsilon} = \mathbf{0.5}$ and of the lamellar structure at larger strain $\bar{\varepsilon} = \mathbf{2.5}$.

$\bar{\varepsilon}$	h	q	$\bar{\sigma}$	$\tilde{h}$	$\tilde{q}$	θ	θ_{roll}	λ
–	[MPa]	–	[MPa]	[MPaμm]	–	–	–	[μm]
0.5	400	1.5	−500	53	6.3	60°	30°	1
2.5	60	1.5	−700	5.7	1.1	85°	5°	0.2

volume V is V/λ. For this profile, the gradient F'' is transformed into the δ-functions at the positions of the GNBs with the shear jump $\pm(2a/\lambda)$. Under these assumptions, the functional (22) integrated over the crystal domain Ω becomes a function written in the reduced form $\bar{J}$

$$\bar{J}(\xi,\lambda) = \frac{2J}{Va^2} = \frac{1}{\lambda^2}\left(4H_{xx}\xi^2 + H_{xy}\left(\xi^2-1\right)^2 - \frac{\bar{\sigma}}{2}\left(1-\xi^4\right)\right) - \frac{1}{\lambda^3}\left(K_1\xi^4 + K_2\left(1-\xi^2\right)^2 + L_1\xi^2 + L_2\xi^2\left(1-\xi^2\right)^2 + M\xi^2\left(\xi^2-1\right)\right) + \frac{Gb}{\lambda^3}\left(4\bar{B}_{xx}\xi^2 + \bar{B}_{xy}\left(\xi^2-1\right)^2\right), \tag{25}$$

where the assumption $h_{bow} = Gb/\lambda$ is accepted and

$$\bar{B}_{xx} = \frac{1}{2\sin^2 2\phi}, \quad \bar{B}_{xy} = \frac{1}{2\cos^2 2\phi}. \tag{26}$$

The condition $\bar{J}(\xi,\lambda) < 0$ determines the rage of the pattern characteristics ξ and λ of the deformation bands which may be formed. The value of $\bar{J}$ can be understood as a measure of the instability growth. The fastest growing instability is indicated by the minimum of $\bar{J}$, which can be evaluated from the condition

$$\frac{\partial\bar{J}(\xi,\lambda)}{\partial\xi^2} = 0, \quad \frac{\partial\bar{J}(\xi,\lambda)}{\partial L} = 0. \tag{27}$$

The minimum of $\bar{J}$ (or infimum) points to the deformation banding which would dominate the forming pattern. However, the condition (27) does not imply the condition $\delta J = 0$, therefore the solution corresponding to the minimum does not need to satisfy the stress equilibrium (12), it only indicates a trend to reach energetically stable state.

We assume that the set of the deformation modes to be optimized is restricted to structures arising from superposition of one or two periodically arranged sets of dominating deformation bands perpendicular to the directions ξ and $-\xi$, Fig. 3. In this Section, a single set of the bands with the orientation ξ is considered.[6] In Section 4, it is proposed that the second set of the bands provides a mechanism of the reorientation of the bands observed at large strains.

4. Results and discussion

The energetic function $\bar{J}(\xi,\lambda)$ expressed in (25) is controlled by the self-hardening h, by the latent-to-self hardening ratio q, by the flow stress $\bar{\sigma}$, by the shear modulus G, by the magnitude of the Burgers vector b, by the boundary slip resistance $\tilde{h}$, and by the slip resistance anisotropy $\tilde{q}$. For a given material at a given strain, h and $\bar{\sigma}$ can be estimated from a stress–strain diagram. At small strains, the value of the ratio q is usually taken $q \sim 1.4$; to our knowledge, for medium and large strains q is not known. It can be only safely assumed that $q > 1$, as for all strains a local decrease of the number of the active slip systems controlled by q is energetically favorable. G and b are known constants, however, the assumption that the line tension strengthening $h_{bow} = Gb/\lambda$ modifies h results from an intuition rather than from a rationally deduced consequence of the bowing mechanism. The reason is that the role of the dislocation cells in the process of deformation banding is not well known yet.

To illustrate the predictive ability of the model, two examples are presented: the deformation bands formed in Ni at a moderate strain $\bar{\varepsilon} = 0.5$ and at a large strain $\bar{\varepsilon} = 2.5$. The examples are presented in Table 1. Let us note that for data presented in Table 1, an additional energy minimum exists at $\xi = 0$, i.e. $\theta_{roll} = 90°$, however, deformation bands perpendicular to the rolling direction do not seem to be observed.

At the moderate strain $\varepsilon = 0.5$, the self-hardening $h = 400$ MPa and the compressive flow stress $\bar{\sigma} = -500$ MPa were deduced for Ni from the stress–strain diagram in Hansen and Jensen (2011) (Fig. 14); for nickel $G \sim 70$ GPa and $b = 0.25$ nm, i.e. $Gb = 17$ MPa μm; we used the hardening anisotropy ratio $q = 1.5$. For the boundary resistance $\tilde{h} = 63$ MPa μm and the resistance anisotropy $\tilde{q} = 6.3$ employed as the fitting parameters, the minimum of the energetic function $\bar{J}$ is reached for $\lambda = \lambda_{min} = 1$ μm and $\xi = 1.7$ corresponding to $\theta = 60°$, i.e. the angle $\theta_{roll} = 30°$ to the rolling direction. The values of the band width λ and the inclination angle θ_{roll} correspond roughly to the measured values presented in Hughes et al. (1999) $\lambda \sim 1.5$ μm

[6] A probable reason that two criss-crossing sets are less frequently observed is an interaction between sets not covered by the present linearized model.

(deduced from the graph Fig. 3 in Hughes et al. (1999)) and the observed $\theta_{roll} \sim 35^\circ$. In the example of the moderate strain, $\tilde{h}$ and $\tilde{q}$ are the factors controlling the orientation and the width of the bands.

At the large strain $\varepsilon = 2.5$, we used the self-hardening $h = 60$ MPa and the compressive flow stress $\overline{\sigma} = -700$ MPa deduced for Ni from Hansen and Jensen (2011) (Fig. 14), and the hardening anisotropy ratio $q = 1.5$. For the boundary resistance $\tilde{h} = 5.7$ MPa μm and the resistance anisotropy $\tilde{q} = 1.1$ employed as the fitting parameters, the minimum of the reduced energetic function $\bar{J}$ is reached at $\lambda = \lambda_{min} = 0.2$ μm and $\xi = 130$ corresponding to $\theta = 85^\circ$, i.e. the angle $\theta_{roll} = 5^\circ$ to the rolling direction. The values of the band width λ and the inclination angle θ_{roll} correspond roughly to the observed trend of a decreasing band width and the reorientation of the bands toward the rolling direction.

Due to several simplifying assumptions, numerical data provided by the model are solely indicative. Table 1 may be understood as an illustrative example. The material parameters and the evolution of the structural characteristics for usually experimentally studied grains of polycrystals or single crystals (Cu, Al, Ni) are an order of magnitude the same. Therefore, it is easy to find values of parameters $\tilde{h}$ and $\tilde{q}$ fitting the structural data as long as they are available. The ambitions of the proposed model are modest. We attempt to interpret the observation sequence of the band structure evolution with increasing strain as described namely in the papers Hughes and Hansen (1993, 2000).

Based on the proposed model, the significant change in the structural morphology with increasing strain, i.e. the reorientation of the bands from $\sim 35^\circ$ to nearly 0° with respect to the rolling direction, can be interpreted as the transition from the boundary control bands formation to the bowing stress control. The change of the boundary resistance characteristics $\tilde{h}$ and $\tilde{q}$ can be understood as a consequence of transformation of the dense dislocation walls (DDWs) of the cell blocks into the microbands. A trend of the boundary resistance to isotropy at large strain, $\tilde{q} \to 1$, contributes to the tendency to orient the deformation bands parallel to the rolling direction $\xi \to \infty$ and to reach a zero width. As a consequence, the controlling factor at the large strain becomes the bowing stress which prevents these extremes. In this context, it is interesting to note that the observed lamellae are never parallel to the rolling direction and their width remains finite (Hughes and Hansen, 1993, 2000). Moreover, the bands of the intensive localized slip (S-bands) as a part of the mechanism of the reorientation of the deformation bands, recalled in Introduction, Fig. 1, can be interpreted as the second set of bands $-\xi$, being complementary to the set of the microbands ξ shown in Fig. 3. The set $-\xi$ provides a suitable and energetically favorable tool for such mechanism. The observed nearly mirror orientation of the S-bands with respect to microbands supports such interpretation. The transformation of the DDWs into the microbands, which according to the interpretation above triggers the band reorientation, is not explained by the proposed model. The explanation is a part of a wider problem of the inner cell structure of the deformation bands. The formation of the inner structure and its cooperation with the deformation banding process, not addressed in the present paper, remains an open problem.

There is an alternative, more common explanation of the reorientation of bands into alignment with the rolling plane at large deformation (Albou et al., 2010; Mahesh, 2015). According to this hypothesis, localized secondary slip intensifies at large strains and intersection of this secondary microshear with pre-existing bands creates immobile pinning points on the band walls. These immobilized walls start undergoing rigid body rotations towards the rolling direction. On the other hand, according to our interpretation, the reorientation is treated as an energy minimization process initiated by the observed transformation of the dense dislocation walls into microbands. Moreover, the scheme in Fig. 1 (reproduced from Hughes and Hansen (1993)) does not indicate any rigid rotation of the bands, it rather demonstrates their transformation.

5. Summary

- The deformation bands (internal buckling) are interpreted as a spontaneously formed dislocation pattern caused by anisotropy induced by the slip nature of plastic deformation.
- The model points to the main constituents which control the fragmentation mechanism: anisotropy of the hardening matrix, anisotropic resistance of the boundaries to slip, and the bowing stress.
- The coefficients $\tilde{h}$ and $\tilde{q}$ representing the energy contribution of the boundaries serve as the fitting parameters. The assumption that the line tension strengthening $h_{bow} = Gb/\lambda$ modifies the self-hardening h is rather intuitive.
- The model in the plain strain approximation of symmetric double slip compression predicts the orientation and width of the bands in favorable agreement with available observations.
- The significant change in the structural morphology with increasing strain, i.e. the reorientation of the bands from $\sim 35^\circ$ to nearly 0° with respect to the rolling direction, is interpreted as the transition from the boundary control bands formation to the bowing stress control. The process is related to the transformation of the dense dislocation walls into microbands. The reorientation is assisted by the bands of intensive localized slip, so-called S-bands. The microbands and the interfering S-bands are interpreted as a pair of ξ and $-\xi$ oriented deformation bands.
- The model provides an analytical solution and a physical insight into the process of deformation banding. The price paid is a number of simplifying assumption employed in the modeling.
- The role of the inner structure of the bands (cells, Taylor lattice), the sharp or diffuse shapes of the boundaries, and the transformation of the dense dislocation walls into the microbands remain open problems.
- The next natural step, including a numerical set-up, would be to introduce multi-slip of a general orientation and to apply the method suggested by Petryk and Kursa (2013). Their second order minimization extended to a finite time step enables a numerical calculation of the initial modes of deformation banding and allows tracing deformation paths which occur

under external control. A term describing the anisotropic resistance of the boundaries to slip and the bowing stress could be added to Petryk-Kurza's approach, as proposed in the present paper.

Acknowledgment

This work was supported by GAČR through project P107/12/0121. JK gratefully appreciates inspiring discussions with Dr. Grethe Winther from Technical University of Denmark.

References

Albou, A., Driver, J., Maurice, C., 2010. Microband evolution during large plastic strains of stable {110}⟨112⟩ All and Al-Mg crystals. Acta Mater. 58, 3022–3034.
Arul Kumar, M., Mahesh, S., 2012. Banding in single crystals during plastic deformation. Int. J. Plast. 36, 15–33.
Arul Kumar, M., Mahesh, S., 2013. Subdivision and microstructure development in f.c.c. grains during plane strain compression. Int. J. Plast. 44, 95–110.
Asaro, R., 1979. Geometrical effects in the inhomogeneous deformation of ductile single crystals. Acta Metall. 27, 445–453.
Asaro, R., 1983. Micromechanics of crystals and polycrystals. Adv. Appl. Mech. 23, 1–115.
Aubry, S., Ortiz, M., 2003. The mechanics of deformation-induced subgrain-dislocation structures in metallic crystals at large strains. Proc. R. Soc. Lond. A 459, 3131–3158.
Bargmann, S., Reddy, B., Klausemann, B., 2014. A computational study of a model of single-crystal strain-gradient viscoplasticity with an interactive hardening relation. Int. J. Solids Struct. 51, 2754–2764.
Bassani, J., 1994. Plastic flow of crystals. Adv. Appl. Mech. 30, 191–258.
Bay, B., Hansen, N., Hughes, D., Kuhlmann -Wilsdorf, D., 1992. Evolution of f.c.c. deformation structures in polyslip. Acta Metall. Material. 40, 205–219.
Biot, M., 1965. Mechanics of Incremental Deformations. John Willey.
Cermelli, P., Gurtin, M., 2001. On the characterization of geometrically necessary dislocations in finite plasticity. J. Mech. Phys. Solids 49, 1539–1568.
Delannay, L., Barnett, M., 2012. Modelling the combined effect of grain size and grain shape on plastic anisotropy of metals. Int. J. Plast. 32–33, 70–84.
Groma, I., Csikor, F., Zeiser, M., 2003. Spatial correlations and higher-order gradient terms in a continuum description of dislocation dynamics. Acta Mater. 51, 1271–1281.
Gurtin, M., Reddy, B., 2014. Gradient single-crystal plasticity within a mises-hill framework based on a new formulation of self- and latent-hardening. J. Mech. Phys. Solids 68, 134–160.
Hansen, N., Jensen, D.J., 2011. Deformed metals – structure, recrystallisation and strength. Mater. Sci. Technol. 27, 1229–1240.
Harren, S., Dève, H., Asaro, R., 1988. Shear band formation in plane strain compression. Acta Metall. 36, 2435–2480.
Hill, R., 1966. Generalized constitutive relations for incremental deformation of metal crystal by polyslip. J. Mech. Phys. Solids 14, 95–102.
Hill, R., Rice, J., 1972. Constitutive analysis of elastic-plastic crystals at arbitrary strain. J. Mech. Phys. Solids 20, 401–413.
Hong, C., Huang, X., Winther, G., 2012. Experimental characterization of dislocations in deformation induced planar boundaries of rolled aluminium. In: S. F, et al. (Eds.), Proceedings of the 33rd Risoe Int. Symposium on Material Science: Nanometals – Status and Perspective. ISSN: 0907-0079. Risoe National Laboratory, Roskilde, Denmark, pp. 239–248.
Huang, X., Winther, G., 2007. Dislocation structures. Part I. Grain orientataion dependence. Philos. Mag. 87, 5189–5214.
Hughes, D., 1993. Microstructural evolution in a non-cell forming metal: Al-Mg. Acta Metall. Material. 41, 1421–1430.
Hughes, D., 2001. Microstruture evolution, slip pattern and flow stress. Mater. Sci. Eng. A 319–321, 46–54.
Hughes, D., Hansen, N., 1993. Microstructural evolution in nickel during rolling from intermediate to large strains. Metall. Trans. A 24, 2021–2037.
Hughes, D., Hansen, N., 2000. Microstructure and strength of nickel at large strains. Acta Mater. 48, 2985–3004.
Hughes, D., 1999. Distribution of low and high angle boundaries in deformed metal. In: Sakai, T., Suzuki, H. (Eds.), Proceedings of the Fourth Conference on Recrystalization and Related Phenomena. The Japan Institute of Metals, pp. 111–118.
Klusemann, B., Kochmann, D.M., 2014. Microstructural pattern formation in finite-deformation single-slip crystal plasticity under cyclic loading: relaxation vs. gradient plasticity. Comput. Methods Appl. Mech. Eng. 278, 765–793.
Klusemann, B., Yalinkaya, T., 2013. Plastic deformation induced microstructure evolution through gradient enhanced crystal plasticity based on a non-convex helmholtz energy. Int. J. Plast. 48, 168–188.
Kratochvíl, J., 1990. Instability origin of dislocation cell misorientation. Scripta Metall. Material. 24, 1225–1228.
Kratochvíl, J., Kružík, M., 2015. A crystal plasticity model of a formation of a deformation band structure. Philos. Mag. A 95, 3621–3639.
Kratochvíl, J., Kružík, M., 2014. A model of deformation bands formation. In: S. F, et al. (Eds.), Proceedings of the 35th Risoe Int. Symposium on Material Science: New Frontiers of Nanometals. Risoe National Laboratory, Roskilde, Denmark, pp. 357–364.
Kratochvíl, J., Orlová, A., 1990. Instability origin of dislocation substructure. Philos. Mag. A 61, 281–290.
Kratochvíl, J., Sedláček, R., 2004. Energetic approach to subgrain formation. Mater. Sci. Eng. A 387–389, 67–81.
Kratochvíl, J., Sedláček, R., 2008. Statistical foundation of continuum dislocation plasticity. Phys. Rev. B 77, 134102 (1997).
Kratochvíl, J., Kružík, M., Sedláček, R., 2007. Statistically based continuous model of dislocation cell structure formation. Phys. Rev. B 75, 064104–064114.
Kratochvíl, J., Kružík, M., Sedláček, R., 2009. A model of ultrafine microstructure evolution in materials deformed by high pressure torsion. Acta Mater. 57, 739–748.
Kuhlmann-Wilsdorf, D., 1999. “Regular” deformation bands (DBs) and the LEDS hypothesis. Acta Mater. 47, 1697–1712.
Leffers, T., 2001. A model for rolling deformation with grain subdivision. Part I: the initial stage. Int. J. Plast. 17, 469–489.
Leffers, T., 2001. A model for rolling deformation with grain subdivision. Part II: the subsequent stage. Int. J. Plast. 17, 491–511.
Mahesh, S., 2006. Deformation banding and shear banding in single crystals. Acta Mater. 54, 4565–4574.
Mahesh, S., 2012. Orientation preferences of extended sub-granular dislocation boundaries. Philos. Mag. 92, 2286–2312.
Mahesh, S., 2015. A minimum principle for microstructuring in rigid-viscoplastic crystalline solids. J. Mech. Phys. Solids 84, 39–58.
Ortiz, M., Repetto, E., 1999. Nonconvex energy minimization and dislocation structures in ductile single crystals. J. Mech. Phys. Solids 47, 397–462.
Ortiz, M., Repetto, E., Stainier, L., 2000. A theory of subgrain dislocation structures. J. Mech. Phys. Solids 48, 2077–2114.
Peirce, D., Asaro, R., Needleman, A., 1983. Material rate dependence and localized deformation in crystalline solids. Acta Metall. 31, 1951–1976.
Petryk, H., 1992. Material instability and strain-rate discontinuities in incrementally non-linear continua. J. Mech. Phys. Solids 40, 1227–1250.
Petryk, H., 2000. General conditions for uniqueness in materials with multiple mechanisms of inelastic deformation. J. Mech. Phys. Solids 48, 367–396.
Petryk, H., Kursa, M., 2011. Selective symmetrization of the slip-system interaction matrix in crystal plasticity. Arch. Mech. 63, 287–310.
Petryk, H., Kursa, M., 2013. The energy criterion for deformation banding in ductile single crystals. J. Mech. Phys. Solids 61, 1854–1875.
Petryk, H., Thermann, K., 2002. Post-critical plastic deformation in incrementally nonlinear materials. J. Mech. Phys. Solids 50, 925–954.
Sedláček, R., 1999. Instability Origin of Subgrain Formation (Ph.D. thesis). University of Erlangen.
Sedláček, R., Kratochvíl, J., 2005. Variational approach to subgrain formation. Z. Met. 96, 602–607.
Sivakumar, S., Ortiz, M., 2004. Microstructure evolution in the equal channel angular extrusion. Comput. Methods Appl. Mech. Eng. 193, 5177–5194.

van Beers, P., McShane, G., Kouznetsova, V., Geers, M., 2013. Grain boundary interface mechanics in strain gradient plasticity. J. Mech. Phys. Solids 61, 2659–2679.

Vattre, A., Devincre, B., Feyel, F., Gatti, R., Groh, S., Jamond, O., Roos, A., 2014. Modeling crystal plasticity by 3D dislocation dynamics and the finite element method. The discrete-continuum model revisited. J. Mech. Phys. Solids 68, 491–505.

Winther, G., Huang, X., 2007. Dislocation structures. Part II. Slip system dependence. Philos. Mag. 87, 5215–5235.

Winther, G., Hong, C., Huang, X., 2014. Comparison of experimental and predicted dislocation network in deformation-induced dislocation boundaries aligned with slip planes in aluminium. In: S. F, et al. (Eds.), Proceedings of the 35rd Risoe Int. Symposium on Material Science: New Frontiers of Nanometals. ISSN: 0907-0079. Department of Wind Energy, Technical University of Denmark, Roskilde, Denmark, pp. 479–484.

Winther, G., 2012. Theoretical analysis of slip-plane-aligned geometrically necessary dislocation boundaries originating from two sets of coplanar slip systems. In: S. F, et al. (Eds.), Proceedings of the 33rd Risoe Int. Symposium on Material Science: Nanometals – Status and Perspective. ISSN: 0907-0079. Risoe National Laboratory, Roskilde, Denmark, pp. 115–128.